radiation damage

Plastic-embedded protein crystals

Raimond B. G. Ravelli,[a]* Uta Haselmann-Weiss,[b] John E. McGeehan,[a] Andrew A. McCarthy,[a] Josan A. Marquez,[a] Claude Antony,[b] Achilleas S. Frangakis[b] and Gudrun Stranzl[a]

[a]EMBL Grenoble, 6 rue Jules Horowitz, BP 181, 38042 Grenoble CEDEX 9, France, and [b]EMBL Heidelberg, Meyerhofstrasse 1, 69117 Heidelberg, Germany. E-mail: ravelli@embl.fr

Rapid vitrification followed by the replacement of the vitrified water by a solvent (freeze substitution) and then resin is a widely used procedure for preparing biological samples for electron microscopy. The resulting plastic-embedded samples permit convenient room-temperature sectioning (microtomy) and can yield well preserved cellular structures. Here this procedure has been applied to crystalline protein samples, and it is shown that it is possible to freeze-substitute vitrified crystals while preserving some of their original diffraction properties. The plastic-embedded crystals were used to collect a series of complete room-temperature data sets at a powerful macromolecular crystallography synchrotron beamline. Whereas one normally observes specific damage to disulfide bonds upon X-ray radiation, no such damage was seen for the plastic-embedded sample. The X-ray diffraction data allowed an initial atomic analysis to be made of the effects of freeze-substitution and plastic embedding on biological samples.

Keywords: radiation damage; freeze substitution; resin embedding.

1. Introduction

Could you imagine that any protein crystal would survive the following treatment? First, the crystal is dehydrated for two and a half days with anhydrous acetone or methanol, followed by four days of gradual replacement of the organic solvent by a resin at an increased temperature. Once all the organic solvent has been replaced, the resin-infiltrated samples are polymerized for four days under UV irradiation. The samples are finally stabilized in the hard resin and are then in a state where they could be mailed to a synchrotron in a normal envelope or taped to a postcard. It sounds like the ideal way to overcome the ever-increasing problems and expenses associated with crystal-storage dewar shipping and airport security.

The only reason why this protocol might possibly work is that it starts with cryo-immobilized samples. Such methods are well established within the field of electron microscopy (EM) for the study of cells or tissue (Steinbrecht, 1993; Giddings *et al.*, 2001; McIntosh, 2001; Edelmann, 2002; Koster & Klumperman, 2003; Matsko & Mueller, 2005). The interest in preparing samples by rapid vitrification followed by the replacement of the vitrified water by a solvent (freeze substitution), fixation and embedding in plastic resin, lies in the increased ease of subsequent sectioning, imaging at room temperature, and improved lifetime in the electron beam. The disadvantage is that plastic-embedded samples are likely to show differences in their macromolecular organization due to the dehydration of the sample compared with samples that did

not undergo any chemical treatment at all (Dubochet *et al.*, 1988). However, plastic embedding has provided specimens suitable for detailed three-dimensional studies of cells (McIntosh, 2001).

Macromolecular crystallography (MX) is rapidly reaching the state, as in EM, where the resolution of the final structure is solely determined by the amount of radiation damage the fragile sample can withstand. Since the introduction of powerful third-generation synchrotron MX beamlines, structural biologists routinely reach the Henderson limit of 2×10^7 Gy, at which the cryo-cooled crystal has lost half of its original crystalline diffractive properties (Henderson, 1990; Owen *et al.*, 2006). Studies to overcome this limit, for example by the use of scavengers (Murray & Garman, 2002; Kauffmann *et al.*, 2006) or the use of open-helium-flow cryo-jets (Hanson *et al.*, 2002), do not yet seem to hold the promise of greatly extending the crystal lifetime. It is therefore pertinent to learn from radiation-damage experiences in electron beam imaging and diffraction, and investigate whether some of the anti-damage approaches used in these fields might be applicable to MX (Massover, 2006).

Here we report the very first experiments on plastic-embedded protein crystals. An EM protocol was slightly modified and tested on tetragonal crystals of lysozyme. Although so far with limited success, it is shown that the plastic-embedded crystals did indeed diffract X-rays, and that complete data sets could be obtained at room temperature on a very bright synchrotron MX beamline. We discuss how the

initial results might be improved and evaluate the promise this sample preparation technique holds for both the fields of MX and EM.

2. Material and methods

2.1. Crystallization

Lyophilized chicken hen egg-white lysozyme (HEWL) from Sigma was dissolved to a concentration of 50 mg ml^{-1} in 50 mM sodium acetate pH 4.5. Crystals with typical dimensions of 250 μm × 250 μm × 200 μm were grown overnight using the sitting-drop vapour diffusion method by mixing 2 μl protein solution with 2 μl reservoir solution containing 1 M NaCl and 100 mM sodium acetate pH 4.5.

2.2. Freeze substitution

Individual crystals were harvested using a Hampton-mounted cryo-loop (www.hamptonresearch.com) and transferred into a cryo-protectant buffer solution containing 30% PEG 400, 1 M NaCl and 100 mM sodium acetate pH 4.5. The crystals were vitrified by dipping the samples in liquid nitrogen (77 K) and subsequently transferred in a freeze-substitution device (AFS Auto, Leica) to a pre-cooled (183 K) Eppendorf tube filled with anhydrous acetone. The samples were freeze-substituted over 55 h at 183 K in anhydrous acetone and subsequently warmed to 228 K at a rate of 5 K h^{-1}. After 70 h, samples were infiltrated with Lowicryl HM20 resin (Polyscience, Warrington, PA, USA) performed through several steps at 228 K: acetone/Lowicryl 3:1 for 1 h, 1:1 for 2–3 h, 1:3 for 2–3 h, pure Lowicryl two times 1 h. Hereafter the samples were left overnight in pure Lowicryl. A last resin change was made before starting the UV polymerization under a 360 nm UV-irradiation at 228 K for 48 h. The samples were subsequently warmed to 293 K at a rate of 10 K h^{-1}, and the polymerization was continued for another 24 h. The Lowicryl-embedded samples are stable at room temperature and ambient humidity. The excess of resin was removed with a blade and samples were epoxy glued to a loopless Hampton magnetic crystal-cap. All crystals were clearly visible within the surrounding transparent resin.

2.3. Data collection and processing

The crystals were screened at room temperature at the high-brilliance MAD (multiple-wavelength anomalous dispersion) beamline ID29 of the European Synchrotron Radiation Facility (ESRF), Grenoble, France (Flot *et al.*, 2006). The beam intensity was attenuated to 5% and X-rays of 0.976 Å wavelength were used. The exposure time per image was 3 s and data were recorded using a 3 × 3 mosaic CCD detector from Area Detector Systems Corporation. The diffraction spots were integrated using *XDS*, merged and scaled using *XSCALE* (Kabsch, 1988), and converted to structure factors using *TRUNCATE* (Collaborative Computational Project, Number 4, 1994).

Most of the eight crystals tested showed a rather high mosaicity and the spot shape was often dependent on the exact position where the 50 μm × 50 μm X-ray beam was incident on the 250 μm × 250 μm × 200 μm-sized crystal. Almost all crystals tested diffracted to similar resolutions; however, not all diffraction patterns could be indexed, probably due to bad spot shapes. A series of three complete data sets (55 frames, 2° per frame) was collected on the best diffracting crystal without translating the crystal between the data sets. The total dose was estimated to be 1 × 10^6 Gy per data set, as calculated using *RADDOSE* (Murray *et al.*, 2004) with an estimated attenuated flux of 4 × 10^{10} photons s^{-1} into 50 μm × 50 μm. We note that as *RADDOSE* does not take any rotation into account, the dose is only valid for the part of the crystal that stays in the beam throughout rotation.

As controls, two additional experiments were carried out on untreated lysozyme crystals. In the first experiment, a crystal was cryo-cooled after cryo-protection (as described in §2.2). Diffraction images were collected at 100, 125, 150, 175 and 200 K, and the diffraction patterns were analysed to give unit-cell constants, crystal mosaicity and ice formation. In the second experiment, cryo-protected crystals were mounted in a cryo-loop and allowed to dehydrate in air for up to 15 h. These crystals were cryo-cooled afterwards and checked for diffraction and unit-cell parameters, as well as for specific damage.

2.4. Structure solution and refinement

The structure was solved using molecular replacement (Vagin & Teplyakov, 1997) with Protein Data Bank (PDB) model 2BLX (Nanao *et al.*, 2005). The structure was refined using the program *REFMAC* employing *TLS* (Winn *et al.*, 2001). Residues 66–75 and 128–129 were omitted from the final model, as these residues were not well defined in σ$_a$-weighted electron density maps (Read, 1986). For the same reason, the following side-chains were mutated to alanines: 1, 5, 7, 8, 12–14, 17–21, 23, 25, 33, 35, 38, 41, 43, 46, 52–53, 56–58, 61, 77, 83–84, 87, 93, 96–98, 105, 109, 112–114, 116, 118–120, 123–125. Maps were inspected and models were improved using the program *COOT* (Emsley & Cowtan, 2004). The program *ESCET* (Schneider, 2002) was used to compare our structure with 2BLX. Difference maps were calculated between successive data sets to check for any visible specific damage (Weik *et al.*, 2000; Ravelli & McSweeney, 2000).

3. Results and discussion

3.1. Crystal morphology and diffraction properties

Fig. 1 shows a plastic-embedded HEWL crystal as seen through the on-axis visualization unit on the ID29 beamline. Almost all crystals tested showed severe cracking, although their original morphology was well preserved. Given these cracks, it was surprising to see any diffraction at all: most crystals had similar diffractive properties and diffracted to 5 Å or better. Table 1 shows the statistics of three successive data sets collected at the same place on the best crystal. Fig. 2 shows a diffraction pattern from this crystal. Most macromolecular crystals would show a water ring around 3.8 Å; however, this

Table 1
Data collection statistics of three successive room-temperature data sets collected from the same volume of a plastic-embedded lysozyme crystal.

Values in parentheses are for the higher-resolution shell (4.47–4.2 Å).

Space group	$P4_32_12$
Unit-cell parameters (Å)	$a = 72.57$, $c = 32.29$
Resolution (Å)	40–4.2
Mosaicity (°)	1.0

	Run 1	Run 2	Run 3
No. of reflections	5166 (797)	5179 (788)	5208 (799)
No. of unique reflections	730 (114)	724 (107)	734 (113)
Completeness (%)	98.8 (100.0)	98.2 (95.5)	99.1 (99.1)
$\langle I/\sigma(I)\rangle$	18.8 (4.3)	16.4 (3.0)	13.4 (2.2)
R-factor (%)†	6.7 (34.7)	7.1 (51.8)	9.0 (70.1)
Redundancy	7.1 (7.0)	7.2 (7.4)	7.1 (7.1)

† R-factor is $\Sigma|I(h,i) - I(h)|/\Sigma I(h)$, where $\Sigma I(h)$ is the intensity of the reflection with index h and $I(h,i)$ is the intensity of the symmetry-related i reflection with index h.
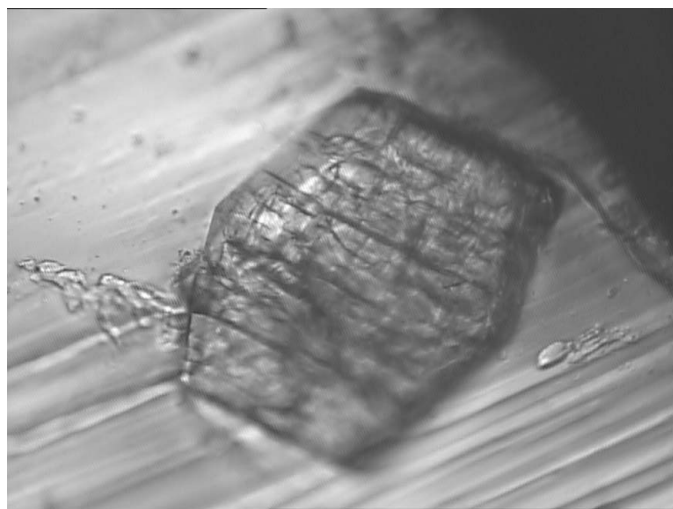

Figure 1
Photograph of a plastic-embedded lysozyme crystal as seen through the on-axis visualization unit of the mini-diffractometer at ID29, ESRF. The crystal has dimensions of 250 μm × 250 μm × 200 μm and is embedded in the polymerized resin.

Figure 2
Diffraction pattern of a plastic-embedded protein crystal. Despite the apparent cracks within the crystal (Fig. 1), a single lattice diffraction pattern could be obtained. The mosaicity was 1.0°. The diffuse-scattering ring comes from the plastic, whereas no diffuse water ring can be observed.

ring is completely absent for our dehydrated crystals. Instead, strong diffuse scattering of the plastic is clearly visible around 4.8 Å. This background scattering made it very hard to collect data to resolutions higher than 4.2 Å and calls for a better removal of the excess of plastic surrounding the crystal. A box of a few mm was cut around the crystal and the excess amount of plastic was used to attach it to the supporting sample holder; this, although practical, was not optimal in terms of background scattering.

Despite the severe macroscopic damage to the crystal, reasonable diffraction spots could be obtained. The overall mosaicity refined to an acceptable 1.0°, far larger than native HEWL crystals (usually in the range 0.05–0.2°), but still much better than anticipated from visual inspection of the crystals. The diffraction pattern did not indicate the presence of distinct multiple crystals; instead it could be well described by that of a single stressed crystal.
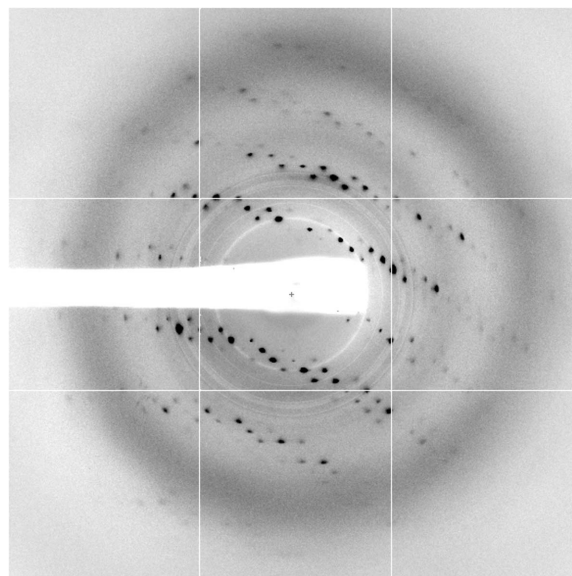
3.2. Solvent content and crystal structure

The unit-cell dimensions of the tetragonal HEWL crystals indicate a very tight packing (Table 1): $a = 72.57$ and $c = 32.29$ Å versus typical dimensions of native crystals at room temperature of $a = 79.27$ and $c = 37.96$ Å (PDB-ID 1BWH; Dong et al., 1999) or $a = 77.32$ and $c = 38.16$ Å for crystals measured at 100 K (PDB-ID 2BLX; Nanao et al., 2005). The measured unit-cell volume of 170050 Å³ indicates a shrinkage of almost 29% compared with the room-temperature unit cell of 1BWH. The Matthews coefficient (Matthews, 1968) of 1.48 Å³ Da⁻¹ corresponds to a solvent content of 17%, versus 41% for 1BWH and 38% for 2BLX. Several studies have been reported on the dynamic response of tetragonal lysozyme crystals to changes in relative humidity. For example, Dobrianov et al. (2001) showed an irreversible unit-cell volume decrease of 9% upon changing the relative humidity around the crystal from 98% to 86%, while Deshpande et al. (2005) showed that dehydratation by organic solvents mainly affected the order of the hydrated waters without causing large changes in the unit-cell dimensions. In our control study, where a lysozyme crystal was allowed to dehydrate in air for 15 h, we measured (100 K) a unit cell of $a = 77.43$ and $c = 37.48$ Å, which corresponds to a solvent content of 37%. The solvent content of the plastic-embedded crystal is by far the smallest value obtained for tetragonal lysozyme (the next lowest solvent content is 35.5%, PDB-ID 1LSB; Kurinov & Harrison, 1995), although, for monoclinic lysozyme, a solvent content as low as 9% has been reported (Nagendra et al., 1998).

The quality of the 4.2 Å electron density was, as expected for this resolution, rather poor; however, helices and disulfide bridges were still well defined. Side-chains were hardly visible,
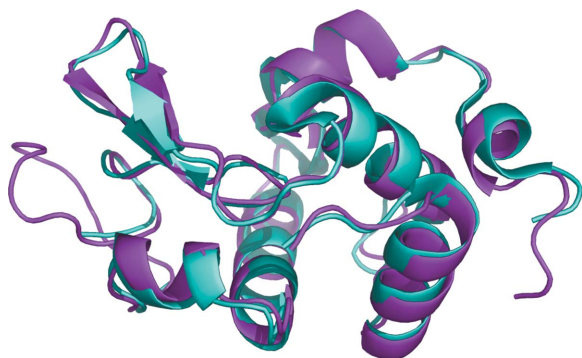
Figure 3
Overlap of lysozyme structures from data obtained from a cryo-vitrified crystal (magenta) *versus* data obtained from a plastic-embedded crystal (cyan). The residues 66–75 (left in figure)and 128–129 (right) were not defined in the electron density of the plastic-embedded crystal.

probably also because of the problems associated with recording the higher-resolution data (higher background and attenuation owing to the plastic surrounding the crystal). Several absorption correction schemes were used, as well as *B*-sharpening of the maps or data. However, these strategies did not result in major improvements in the refined model *R* values. Waters were obviously not visible at this resolution and were excluded from the model. Loop 66–75 had to be excluded as its original conformation would cause severe overlap with a symmetry-related molecule (Fig. 3). No new alternative conformation was found. The excluded residues 66–75 and 128–129 corresponded to the same range of residues that showed large deviation peaks while comparing lysozyme in water and in 90% acetonitrile (Wang *et al.*, 1998). The combined observation of unit-cell shrinkage and loss of density for parts of the molecule might indicate partial unfolding of the cryo-cooled protein. A comparison of our structure with PDB-ID 2BLX (Fig. 3) did not show significant secondary structure domain movements within the molecule.

3.3. Resistance to radiation damage

It is extraordinary that complete data sets could be obtained at room temperature from a protein crystal on the high-flux undulator MX beamline ID29 at the ESRF. A comparison of the data statistics does show a clear crystal decay between the successive data sets (Table 1). Thus plastic embedding of the protein crystal did not bestow immortality to its diffractive lifetime; however, it greatly extended it. The estimated dose per data set is 1×10^6 Gy; the dose used to collect the three room-temperature data sets is about 15% of the Henderson limit (Henderson, 1990; Owen *et al.*, 2006) for cryogenically cooled crystals. This is a >10 times increase compared with the lifetime of room-temperature crystals, which is estimated to be 70–100 less than cryo-cooled ones (Nave & Garman, 2005).

The intensity differences between data sets 1 *versus* 2, and 1 *versus* 3 are 7.6 and 14.0%, respectively, as calculated using the program *SCALEIT* (Collaborative Computational Project, Number 4, 1994). These differences are largely related to global changes, since $F^{\text{obs}}(i) - F^{\text{obs}}(j)$ difference maps do not show major peaks. Earlier studies have shown specific damage

to all disulfide bonds in lysozyme, both at 100 K (Ravelli & McSweeney, 2000; Weik *et al.*, 2000) and room temperature (Helliwell, 1988). In our maps the disulfide bonds remain among the best defined areas of the electron density maps, and no specific damage could be seen on these bonds at all. This might be due to several reasons, such as the absence of water, the role of the resin as a scavenger, or the tighter packing within the crystal. The data from the control study, in which a crystal was dehydrated in air, still showed clear damage to each of the disulfide bonds. We hypothesize that the presence of water plays a crucial role in disulfide rupture upon X-ray irradiation of normal protein crystals.

4. Future perspectives and conclusion

It is possible to freeze-substitute a three-dimensional protein crystal and embed it in resin while preserving some of its original diffraction quality. This proof of principle justifies further work, where problems such as unit-cell shrinkage and crystal cracking need to be overcome.

Freeze-drying, freeze-substitution and resin embedding are now well known techniques that have been used by electron microscopists for more than 25 years (Edelmann, 1978; Steinbrecht & Mueller, 1987). Experience has been obtained in how each of the different steps, *i.e.* vitrification, dehydratation, re-crystallization during freeze-substitution, stabilization by fixatives, interaction with embedding resins and UV irradiation, affect the final structural appearance of the biological sample (Matsko & Mueller, 2005). However, despite its use in obtaining high-quality transmission EM images, many relevant questions concerning freeze-substitution and subsequent embedding remain unanswered. A refined protocol to obtain better-diffracting plastic-embedded lysozyme crystals, as well as well diffracting plastic-embedded crystals of other proteins, could provide detailed insight into some of these questions. For example, the question of whether hydration layers are preserved during freeze-substitution could be answered directly if higher-resolution data could be obtained. Furthermore, the detailed effects that a particular epoxy resin might have on a certain protein could be studied at atomic resolution, once well diffracting plastic-embedded protein crystals are obtained.

The cracks observed in our crystals are unlikely to be due to the vitrification, as the suitability of the cryo-protection protocol utilized was verified on the beamline. One possible cause of the cracking might have been the crystallization of water within the solvent channels of the cryo-cooled crystal while raising its temperature. However, Weik *et al.* (2004) have investigated the solvent behaviour in tetragonal HEWL crystals as a function of temperature, and found that the solvent within these crystals does not crystallize in the temperature range 100–220 K. We confirmed their findings in a separate control experiment (see §2.3) where diffraction patterns were collected on a cryo-cooled native crystal at 100, 125, 150, 175 and 200 K. No cracks became visible whereas the mosaicity only increased moderately from 0.38 to 0.45° and there was no clear sign of ice formation. This makes lysozyme

a favourable test candidate, as most other macromolecular crystals have larger solvent channels and are likely to show a glass transition and ice rings in the diffraction pattern at temperatures well below 220 K (Weik, 2003; Weik *et al.*, 2005). We thus believe that the cracks that can be seen in Fig. 1 were not formed during warming of the sample to 183 K.

The dehydration can either be achieved in anhydrous acetone or methanol, which have comparable melting points of 179 and 175 K, respectively. Although methanol is more hydroscopic, it also acts faster and could cause damage to molecular and cell structures; here we used anhydrous acetone instead. Nevertheless, we still observed damage to the crystals. The huge shrinkage of the unit cell might very well have caused the cracks and could have originated from the dehydration. Electron microscopists often use a fixative to prevent large structural changes as well as aggregation of proteins during dehydration. Aldehyde fixation has successfully been used both by EM (Johnson, 1985) and MX (Fitzpatrick *et al.*, 1994; Wang *et al.*, 1998; Heras & Martin, 2005) and might have been useful to mitigate some of the unit-cell shrinkage we observed. Electron microscopists also use heavy metal staining such as uranyl acetate or osmium tetroxide to enhance the contrast in the EM scope. However, these were omitted in our study as they would greatly increase the absorption of the X-rays (Murray *et al.*, 2004) by the sample.

The protocol after freeze-substitution was identical to that used by cell biologists and therefore it might be possible to improve it for protein crystals. The harvesting of the plastic-embedded crystals would benefit from a better trimming and mounting protocol, and could ultimately be optimized using a microtome or UV laser (Kitano *et al.*, 2005).

A clear drawback of resin-embedding is the need of specialized equipment as well as the two-week preparation period. However, many samples can be prepared in parallel, and the potential rewards, both for macromolecular crystallographers and electron microscopists, could be very real.

References

Collaborative Computational Project, Number 4 (1994). *Acta Cryst.* D**50**, 760–763.

Deshpande, A., Nimsadkar, S. & Mande, S. C. (2005). *Acta Cryst.* D**61**, 1005–1008.

Dobrianov, I., Kriminski, S., Caylor, C. L., Lemay, S. G., Kimmer, C., Kisselev, A., Finkelstein, K. D. & Thorne, R. E. (2001). *Acta Cryst.* D**57**, 61–68.

Dong, J., Boggon, T. J., Chayen, N. E., Raftery, J., Bi, R.-C. & Helliwell, J. R. (1999). *Acta Cryst.* D**55**, 745–752.

Dubochet, J., Adrian, M., Chang, J. J., Homo, J. C., Lepault, J., McDowall, A. W. & Schultz, P. (1988). *Q. Rev. Biophys.* **21**, 129–228.

Edelmann, L. (1978). *Microsc. Acta Suppl.* pp. 166–174.

Edelmann, L. (2002). *J. Microsc.* **207**, 5–26.

Emsley, P. & Cowtan, K. (2004). *Acta Cryst.* D**60**, 2126–2132.

Fitzpatrick, P. A., Ringe, D. & Klibanov, A. M. (1994). *Biochem. Biophys. Res. Commun.* **198**, 675–681.

Flot, D., Gordon, E. J., Hall, D. R., Leonard, G. A., McCarthy, A., McCarthy, J., McSweeney, S., Mitchell, E., Nurizzo, D., Ravelli, R. G. B. & Shepard, W. (2006). *Acta Cryst.* D**62**, 65–71.

Giddings, T. H. Jr, O'Toole, E. T., Morphew, M., Mastronarde, D. N., McIntosh, J. R. & Winey, M. (2001). *Methods Cell Biol.* **67**, 27–42.

Hanson, B. L., Harp, J. M., Kirschbaum, K., Schall, C. A., DeWitt, K., Howard, A., Pinkerton, A. A. & Bunick, G. J. (2002). *J. Synchrotron Rad.* **9**, 375–381.

Helliwell, J. R. (1988). *J. Cryst. Growth*, **90**, 259–272.

Henderson, R. (1990). *Proc. R. Soc. London Ser. B*, **241**, 6–8.

Heras, B. & Martin, J. L. (2005). *Acta Cryst.* D**61**, 1173–1180.

Johnson, T. J. A. (1985). *J. Electron Microsc. Tech.* **2**, 129–138.

Kabsch, W. (1988). *J. Appl. Cryst.* **21**, 916–924.

Kauffmann, B., Weiss, M. S., Lamzin, V. S. & Schmidt, A. (2006). *Structure*, **14**, 1099–1105.

Kitano, H., Murakami, S., Adachi, H., Matsumura, H., Takano, K., Inoue, T., Mori, Y., Doi, M. & Sasaki, T. (2005). *J. Biosci. Bioeng.* **100**, 50–53.

Koster, A. J. & Klumperman, J. (2003). *Nat. Rev. Mol. Cell Biol. Suppl.* pp. SS6–10.

Kurinov, I. V. & Harrison, R. W. (1995). *Acta Cryst.* D**51**, 98–109.

McIntosh, J. R. (2001). *J. Cell Biol.* **153**, F25–32.

Massover, W. H. (2007). *J. Synchrotron Rad.* **14**, 116–127.

Matsko, N. & Mueller, M. (2005). *J. Struct. Biol.* **152**, 92–103.

Matthews, B. W. (1968). *J. Mol. Biol.* **33**, 491–497.

Murray, J. & Garman, E. (2002). *J. Synchrotron Rad.* **9**, 347–354.

Murray, J. W., Garman, E. F. & Ravelli, R. B. G. (2004). *J. Appl. Cryst.* **37**, 513–522.

Nagendra, H. G., Sukumar, N. & Vijayan, M. (1998). *Proteins*, **32**, 229–240.

Nanao, M. H., Sheldrick, G. M. & Ravelli, R. B. G. (2005). *Acta Cryst.* D**61**, 1227–1237.

Nave, C. & Garman, E. F. (2005). *J. Synchrotron Rad.* **12**, 257–260.

Owen, R. L., Rudino-Pinera, E. & Garman, E. F. (2006). *Proc. Natl. Acad. Sci. USA*, **103**, 4912–4917.

Ravelli, R. B. G. & McSweeney, S. M. (2000). *Struct. Fold Des.* **8**, 315–328.

Read, R. (1986). *Acta Cryst.* A**42**, 140–149.

Schneider, T. (2002). *Acta Cryst.* D**58**, 195–208.

Steinbrecht, R. A. (1993). *Microsc. Res. Tech.* **24**, 488–504.

Steinbrecht, R. A. & Mueller, M. (1987). *Cryotechniques in Biological Electron Microscopy*, edited by R. A. Steinbrecht and K. Zierolds, pp. 149–172. Berlin: Springer-Verlag.

Vagin, A. & Teplyakov, A. (1997). *J. Appl. Cryst.* **30**, 1022–1025.

Wang, Z., Zhu, G., Huang, Q., Qian, M., Shao, M., Jia, Y. & Tang, Y. (1998). *Biochim. Biophys. Acta*, **1384**, 335–344.

Weik, M. (2003). *Eur. Phys. J. E*, **12**, 153–158.

Weik, M., Ravelli, R. B. G., Kryger, G., McSweeney, S., Raves, M. L., Harel, M., Gros, P., Silman, I., Kroon, J. & Sussman, J. L. (2000). *Proc. Natl. Acad. Sci. USA*, **97**, 623–628.

Weik, M., Schreurs, A. M., Leiros, H. K., Zaccai, G., Ravelli, R. B. G. & Gros, P. (2005). *J. Synchrotron Rad.* **12**, 310–317.

Weik, M., Vernede, X., Royant, A. & Bourgeois, D. (2004). *Biophys. J.* **86**, 3176–3185.

Winn, M. D., Isupov, M. N. & Murshudov, G. N. (2001). *Acta Cryst.* D**57**, 122–133.